Journal of Molecular Spectroscopy 330 (2016) 4–13

Contents lists available at ScienceDirect

Journal of Molecular Spectroscopy

journal homepage: www.elsevier.com/locate/jms

The extended Lennard-Jones potential energy function: A simpler model for direct-potential-fit analysis

Photos G. Hajigeorgiou

Centre for Primary Care and Population Health, School of Medicine, University of Nicosia, 21 Ilia Papakyriakou, Engomi, P.O. Box 24005, 1700 Nicosia, Cyprus

ARTICLE INFO

Article history:
Received 13 May 2016
In revised form 28 June 2016
Accepted 30 June 2016
Available online 1 July 2016

Keywords:
Extended Lennard-Jones potential
Analytical diatomic potential
Direct-potential-fit
Oxygen
Carbon monoxide
Hydrogen fluoride

ABSTRACT

An analytical model for the diatomic potential energy function that was recently tested as a universal function (Hajigeorgiou, 2010) has been further modified and tested as a suitable model for direct-potential-fit analysis. Applications are presented for the ground electronic states of three diatomic molecules: oxygen, carbon monoxide, and hydrogen fluoride. The adjustable parameters of the extended Lennard-Jones potential model are determined through nonlinear regression by fits to calculated rovibrational energy term values or experimental spectroscopic line positions. The model is shown to lead to reliable, compact and simple representations for the potential energy functions of these systems and could therefore be classified as a suitable and attractive model for direct-potential-fit analysis.

© 2016 Elsevier Inc. All rights reserved.

1. Introduction

The determination of a potential energy function (PEF) for a diatomic molecule from experimental information has long been a principal objective of molecular physics. During the era preceding and following the dawn of quantum mechanics by Heisenberg's matrix mechanics formulation in late 1925 [1], and through Schrödinger's wave mechanics representation in late 1926 [2], simple few-parameter closed-form PEFs were proposed by several investigators [3–6]. The concept of a PEF for an isolated non-interacting electronic state also emerges naturally from the theoretical treatment of Born and Oppenheimer [7], where separation of nuclear and electronic motions is achieved by assuming instantaneous adjustment of the electronic cloud in response to small changes in the internuclear spacing. Essentially, the electronic energy eigenvalues are calculated at fixed internuclear separations, and together with the nucleus-nucleus Coulombic repulsion term they comprise the traditional PEF. Generation of a PEF for a diatomic molecule is an efficient way to encapsulate the rovibrational energy levels and associated wavefunctions, and is particularly useful for further applications in chemical physics.

Owing to limited computational resources and given the relatively crude precision of spectroscopic information at the time, the simple available models for the potential energy were often adequate. However, over the years, the development of more advanced spectroscopic techniques and the associated improvement in the precision of spectroscopic data, along with the parallel enhancement of computational resources, led to the proposal of more refined schemes for the determination of a PEF. A numerical procedure that served as a reliable workhorse for many decades is the Rydberg-Klein-Rees (RKR) method [8–10], which is based on the 1st-order Wentzel-Kramers-Brillouin (WKB) quantization condition [11–13], a convenient framework leading to the solution of the Schrödinger equation for nuclear motions.

The wide availability of powerful microcomputer systems in recent decades has revolutionized the field of spectroscopic analysis. Estimation of molecular constants has been superseded by modern numerical methods, such that direct determination of multi-parameter PEFs from very highly precise spectroscopic data has nowadays become routine. A brief history of the evolution of advanced empirical models for the potential energy is considered below in this article. It is argued that while investigators have achieved superb modeling of the physical aspects of diatomic molecular electronic states, the increasing complexity of the models has rendered the end-products of such work far too unpalatable for most users. As an indication of the growing complexity of modern semi-empirical PEFs, it is worth emphasizing that key contributors to this type of analysis such as Coxon and Hajigeorgiou [14] and Le Roy's group [15] have recently included in supplementary material stand-alone Fortran subroutines for calculating the PEFs from sets of estimated parameters. The principal objective of the present work is to revert to a more comfortable level of simplicity

E-mail address: Hajigeorgiou.p@unic.ac.cy

http://dx.doi.org/10.1016/j.jms.2016.06.014
0022-2852/© 2016 Elsevier Inc. All rights reserved.

in the PEF while still accounting for the various effects that govern the behavior of a chemical bond at different internuclear distances.

The PEF model proposed in the present work is a modified version of the Extended Lennard-Jones (ELJ) potential developed by Hajigeorgiou [16]. The ELJ model is applied in direct-potential-fit (DPF) analyses of three diatomic data sets: (a) rovibrational term values for the ground electronic state of oxygen, (b) a large set of spectroscopic line positions for the ground electronic state of carbon monoxide, and (c) all the available ground state pure rotational, vibrational-rotational and $B \rightarrow X$ electronic data for hydrogen fluoride. It is demonstrated that application of the ELJ model gives results that are fully comparable with those from previous analyses that employed either more complicated or structurally less adequate models for the PEF. The underlying simplicity of the ELJ model makes it a desirable option for DPF analysis.

2. Evolution of PEF models for DPF analysis

The first investigation employing a DPF analysis on diatomic systems was carried out in 1988 by Gruebele et al. on the ground electronic states of the cations OH^+ and ArH^+ [17]. The models selected to represent the PEFs included the Dunham potential polynomial expansion [18], the Simons-Parr-Finlan (SPF) potential polynomial expansion [19], and a Morse potential expansion similar to that proposed originally in Dunham's seminal paper [18]. While all three expansions gave asymptotically well-behaved functions, they failed to adhere to the theoretically expected ion-dipole C_4/r^4 dependence at long-range, which was in any case inconsequential since the spectroscopic data employed did not reach into the long-range region.

In 1990, Coxon and Hajigeorgiou [20] proposed the Generalized Morse Oscillator (GMO) model in the representation of numerical potential energy points, and employed this function successfully in subsequent DPF analyses on a variety of diatomic molecular states [21–23]. The basic structure of the GMO function was that of a Morse potential that incorporated a radial variation on the exponential parameter β. While this PEF form was successful at representing spectroscopic data to within the estimated experimental uncertainties, it had a built-in flaw that could lead to pathological behavior of a PEF extrapolated to large-r beyond the range of the experimental data, if the last fitted parameter of the $\beta(r)$ expansion was fortuitously negative. In addition, even in the case of no pathological behavior, the long-range potentials did not follow well-known theoretical behavior. Owing to these two important limitations, the GMO function does not possess the capability for reliable extrapolation to higher energies.

A more robust PEF was proposed by Dulick in 1993, in a series of publications from the Bernath group employing DPF methodology [24–26]. The modified Morse Oscillator (MMO) model served well in cases where the experimental data did not extend close to the dissociation limit of the potential well. In 1994, Hajigeorgiou and Le Roy [27] proposed a PEF model that simulated the expected long-range asymptotic behavior [28],

$$V(r) = \mathcal{D}_e - C_n/r^n. \tag{1}$$

where $\mathcal{D}_e$ is the dissociation energy of an electronic state, and C_n is the dispersion energy coefficient of the leading r^{-n} term in the long-range potential. The power n is determined with reference to the dissociation products of the electronic state in question. The modified Lennard-Jones (MLJ) model [29] was shown to possess the flexibility to represent effortlessly experimental information that reached up to 99% of the well depth in energy, in contrast to the MMO model, which was shown to lack adequate flexibility at higher energies. The MLJ model was employed successfully in a number of DPF analyses [30–34].

The next significant phase in the evolution of PEFs for DPF analyses was the development in 2006 (publication appeared in 2007) by Le Roy and Henderson [35] of the Morse/Long-Range (MLR) potential function that included extended long-range behavior. The MLR function was capable of modeling the multi-term long-range expansion [36],

$$V(r) = \mathcal{D}_e - C_{n_1}/r^{n_1} - C_{n_2}/r^{n_2} - \ldots, \tag{2}$$

and the model was employed in many subsequent DPF analyses [37–42]. In 2010, Coxon and Hajigeorgiou [43] undertook an extensive DPF analysis of the ground electronic state of the cesium dimer, Cs_2. These authors proposed a slightly modified and more flexible version of the MLR model, and labelled it the MLR3 model. The MLR3 model was highly successful at representing the experimental spectroscopic information available on the ground electronic state of Cs_2, but it integrated an extra degree of complication that required more time-consuming testing at the fitting stage.

The implementation of physically sound long-range behavior in PEF models according to Eq. (2) was discovered to lead to problems on the inner-limb, particularly when higher-order inverse-power dispersion energy terms were included. In order to resolve this problem, Le Roy et al. [44] proposed the inclusion of conventional dispersion term damping functions that reduced the effect of these terms on the short-range behavior of MLR-type functions. Although this eradicated the problems on the inner limb of the derived PEFs, it introduced further complexity in the PEF models. Damping functions were also employed in the recent analysis of hydrogen halide ground electronic states by Coxon and Hajigeorgiou [14] employing an analogously modified MLR3 model. By this stage in the development of PEFs for DPF work, it was felt necessary to provide in supplementary materials computer code for restituting the relevant radial functions, as it was clear that the PEF models had become somewhat unwieldy, such that significant effort and time would be required for PEF calculations by the average user. The extra degree of complexity also introduced additional parameters to the model. The increased sophistication appeared essential in order to model the physical behavior of the PEF to a high degree of accuracy and realism, albeit at the heavy cost of reduced simplicity.

In summary, then, analytical PEF models started with very simple flexible mathematical forms, but became progressively more complicated in order to simulate more realistically the various characteristics of the physics of a chemical bond. This defeated the primary purpose of employing fully analytical PEF models, and could be considered an unwelcome shortcoming of current DPF methodology. In the next two sections, where the ELJ model is described and tested, it is shown that it is possible to fit highly precise experimental spectroscopic information to a PEF that has a more satisfying level of simplicity than currently employed models.

3. The ELJ potential energy function

In 2010, Hajigeorgiou [16] proposed a simple modification of the classic $(2n,n)$ Lennard-Jones function by allowing for a radial variation of the normally constant power n, as in

$$V(r) = \mathcal{D}_e\left[1 - \left(\frac{r_e}{r}\right)^{n(r)}\right]^2, \tag{3}$$

where r_e is the equilibrium internuclear separation. The radial function $n(r)$ is herein modeled as,

$$n(r) = \left(\sum_{i=0}^{N}\rho_i\zeta^i\right)f_n(r) + n_1(1 - f_n(r)), \tag{4}$$

defined with the switching function,

$$f_n(r) = [1 + \exp(\delta_n(r - R_n))]^{-1}, \quad (5)$$

where δ_n controls the rate of switching, and R_n is the internuclear distance at which the switching is half completed. In Eq. (4), ζ is a dimensionless radial coordinate variable such as the Dunham $\xi = (r - r_e)/r_e$ variable [18], or the Ogilvie-Tipping $z = 2(r - r_e)/(r + r_e)$ variable [45], and n_1 is the power of the leading inverse-power term in Eq. (2). In practice it is found that the Dunham variable provides improved economy and flexibility but less stability, whereas the Ogilvie-Tipping variable generally displays better stability but reduced economy. Manual adjustment of the parameters δ_n and R_n is carried out to minimize the standard deviation of the fit, but this is not excessively time-consuming. A reasonable initial estimate of R_n is the classical outer turning point corresponding to the highest vibrational level sampled in the experimental data. A sensible initial estimate of δ_n falls in the range δ_n = 10–15, and this quantity is manually adjusted during the fitting stage as explained above. Reliable initial estimates of the ρ_i parameters in Eq. (4) are furnished by a nonlinear least-squares fit to an available RKR potential.

While the model described by Eqs. (3)–(5) ensures correct qualitative radial behavior at long-range, it does not incorporate known estimates of the dispersion energy coefficients and is thus not quantitatively consistent with Eq. (2). A further modification is possible in order to achieve this goal, giving,

$$V(r) = \mathcal{D}_e\left[1 - C(r)\left(\frac{r_e}{r}\right)^{n(r)}\right]^2, \quad (6)$$

where the long-range radial function $C(r)$ can be written as,

$$C(r) = \left(1 - \frac{f_{LR}(r)}{f_{LR}(r_e)}\right)\left(\frac{1}{2\mathcal{D}_e}\right)\sum_{i=1}^{M}\frac{C_{n_i}}{r_e^{n_i}}\left(\frac{r_e}{r}\right)^{\Delta n} + \frac{f_{LR}(r)}{f_{LR}(r_e)}, \quad (7)$$

where $\Delta n = n_i - n_1$. As an example, for a three-term summation with a leading C_6/r^6 term, $C(r)$ can be written as,

$$C(r) = \left(1 - \frac{f_{LR}(r)}{f_{LR}(r_e)}\right)\left(\frac{1}{2\mathcal{D}_e}\right)\left(\frac{C_6}{r_e^6} + \frac{C_8}{r_e^8}\left(\frac{r_e}{r}\right)^2 + \frac{C_{10}}{r_e^{10}}\left(\frac{r_e}{r}\right)^4\right) + \frac{f_{LR}(r)}{f_{LR}(r_e)}, \quad (8)$$

and can easily incorporate as many dispersion energy terms as desired without any ill-effects on the inner-limb behavior. The radial switching function $f_{LR}(r)$, which can be thought of as an empirical damping function, can be written as,

$$f_{LR}(r) = [1 + \exp(\delta_{LR}(r - R_{LR}))]^{-1}, \quad (9)$$

and the ratio $f_{LR}(r)/f_{LR}(r_e)$ ensures that the $C(r)$ term has a value of unity at $r = r_e$ so as to satisfy the physical/mathematical requirements for a well-behaved PEF, as well as to minimize any perturbing effects of the PEF model on the fitted equilibrium internuclear separation. The parameter δ_{LR} is related to the rate of switching, and R_{LR} is the value of the internuclear separation where the switching is half completed. The initial estimate of R_{LR} is normally selected to be a little smaller (~0.1 to 0.2 Å) than the well-known Le Roy radius [46], and both δ_{LR} and R_{LR} are varied manually in order to minimize the standard deviation of the fit. Reasonable initial estimates of the quantity δ_{LR} fall in the range δ_{LR} = 5–10.

In order for the ELJ model to represent the long-range forces accurately, it is important that $n(r)$ in Eq. (4) be fully switched to n_1 before $C(r)$ is fully switched. This ensures that $V(r)$ converts successfully to the expression Eq. (2) in the long-range region.

Finally, it is sometimes found in practice that the relatively high powers N employed in Eq. (4) may produce unrealistic behavior in the $n(r)$ function at short-r. This can be dealt with in one of two ways: (a) by employing different maximum powers N_I and N_O for the inner and outer limbs, respectively, or (b) by directly controlling the behavior of $n(r)$ below a certain cutoff internuclear distance R_c, adopting a simple slowly-varying mathematical model in this region. The latter approach has been employed successfully in past work [33,34]. Both methods were tested and the second proved more satisfactory, and was thus adopted in all subsequent applications. The first method introduced excessive time-consuming testing, and generally the inner limb representation was found to require polynomial orders that were still high enough to cause problems at short-r. The simple model selected to represent $n(r)$ below R_c is given by,

$$n(r) = ae^{br} \quad \text{for } r \leqslant R_c \quad (10)$$

and the parameters a and b are estimated uniquely by considering the values of $n(R_c)$ and $n'(R_c)$ as determined from Eq. (4) and its first derivative with respect to r. Although this introduces discontinuities in the second and higher derivatives of $n(r)$ and $V(r)$ at $r = R_c$, this was not found to affect adversely the stability of the least-squares fits.

The first derivatives of the Jacobian matrix required for the non-linear least-squares analysis are obtained using a simple 5-point finite-difference method. This is not as optimal in terms of execution time as the use of the Hellmann-Feynman theorem (see for example Ref. [33]), but it allows for frequent changes in the models without the need to derive analytical expressions for the derivatives $\partial V(r)/\partial p_k$ in terms of fitting parameters p_k.

4. Applications

4.1. The ground $X^3\Sigma_g^-$ electronic state of O_2

The set of rovibrational term values employed by Hajigeorgiou [47] to generate a PEF for the ground $X^3\Sigma_g^-$ electronic state of $^{16}O_2$ has been employed in the present work as the first test case for determining an ELJ potential for this molecule. These term values were obtained by subtraction of the spin-spin and spin-rotation contributions, so that they correspond to the simple mechanical terms as expressed by the power series,

$$E_{vN} = G_v + B_vN(N+1) - D_v[N(N+1)]^2 + H_v[N(N+1)]^3, \quad (11)$$

and they extend over vibrational levels with $v = 0$—31, covering approximately 90% of the potential well depth. The PEF was generated in the interval 0.75 Å $\leqslant r \leqslant$ 2.75 Å using a mesh size of 0.0005 Å. The inner and outer classical turning points for $v = 31$ are 0.95 Å and 2.03 Å, respectively. In addition to obtaining a PEF for this electronic state, a radial function $\alpha(r)$ that modifies the conventional rotational operator as in,

$$B(r) = \frac{\hbar^2}{2\mu}\left[\frac{1 + \alpha(r)}{r^2}\right]N(N+1), \quad (12)$$

was included in the Hamiltonian operator, as discussed in Ref. [47]. The value of $\hbar^2/2$ in spectroscopic units employed in all work is 16.85762920 u Å^2. According to theoretical arguments [48], $\alpha(r)$ is expected to vanish at the dissociation limit. As such, this function is dampened using a switching function approach, as in,

$$\alpha(r) = \left(\sum_{i=0}^{N}\alpha_i\zeta^i\right)f_\alpha(r), \quad (13)$$

where

$$f_\alpha(r) = [1 + \exp(\delta_\alpha(r - R_\alpha))]^{-1}. \quad (14)$$

An initial estimate of the pivot point R_α can be obtained with reference to the classical outer turning point of the highest vibrational level sampled in the experimental data, and the initial

damping strength parameter estimate can be in the range δ_α = 5–10. Subsequently, R_α is gradually decreased until it is found to have a measurable increasing effect on the standard deviation of the fit. Finally, δ_α is adjusted systematically in order to minimize the standard deviation of the fit.

The standard deviation achieved in the fit was σ = 0.00070 cm^{-1}, which can be compared with the analogous value of σ = 0.0031 cm^{-1} reported in Ref. [47]. It is considered that the much improved standard deviation is not only due to the new ELJ representation; in the present work, it was possible to obtain an improved mathematical representation for the $\alpha(r)$ radial function and inclusion of extra terms was supported statistically, as ascertained by the ratios of the α_i parameters to their estimated standard errors, which were all significantly greater than unity, and led to a gradual decrease in the standard deviation. This was not possible for the fit in Ref. [47]. The ELJ/$\alpha(r)$ parameter set from the unweighted nonlinear least-squares fit is given in Table 1. The set of constrained parameters for all three applications is given later below in Table 4. Fig. 1 shows the $n(r)$ function, and Fig. 2 shows the $\alpha(r)$ function, the latter being compared with the function reported in Ref. [47]. The two $\alpha(r)$ functions have the same general shape but differ significantly in magnitude. It is considered that the present function is an improved representation, leading to a significantly lower standard deviation. Although the $n(r)$ function displays a small maximum near r = 2.3 Å, there is no corresponding maximum in the $V(r)$ function at similar internuclear distances. The presence of a maximum in the $n(r)$ function is not an unnatural artefact of the least-squares fit. Increasing the switching function strength to reduce the maximum feature led to much worsening of the standard deviation of the fit. Although the outer classical turning point for υ = 31, the highest observed vibrational level, is near r = 2.0 Å, the radial wavefunction of this level is still of significant magnitude in the vicinity of the maximum in $n(r)$, and therefore the maximum feature affects significantly eigenvalue calculations in this region. The $n(r)$ function can be readily calculated where reliable PEF data exist, and it is found that for some electronic states, as for example for the ground $X^1\Sigma_g^+$ electronic state of Cl_2, a well-defined maximum in $n(r)$ does indeed exist. The reason for this phenomenon is discussed later on. For the present case, the $n(r)$ function was represented by a power series in the Ogilvie-Tipping z variable and the $\alpha(r)$ function in terms of a polynomial in the Dunham ξ variable. Fig. 3 shows the potential difference function $\Delta V(r)$ between the present work and Ref. [47]. It is emphasized that the simplistic Morse-like function employed in Ref. [47] did not obey the theoretically predicted long-range form for the potential, whereas the present function applies Eq. (15), below. Thus, at r = 1.9 Å, the potential difference function in Fig. 3 peaks at around 225 cm^{-1}. The accompanying negative difference at short-r is a natural compensating behavior expected so that the pure vibrational eigenvalues are reproduced precisely.

The long-range region was represented by the expression,

$$V(r) = \mathcal{D}_e - \frac{C_6}{r^6} - \frac{C_8}{r^8} - \frac{C_{10}}{r^{10}}, \qquad (15)$$

using the estimate C_6 = 75,182 Å^6 cm^{-1} from Ref. [49]. The values $C_8 = 1.14 \times 10^5$ Å^8 cm^{-1} and $C_{10} = 1.97 \times 10^5$ Å^{10} cm^{-1} were estimated using standard formulas [50].

Table 1
ELJ potential parameters for the $X^3\Sigma_g^-$ electronic state of O_2.

Parameter	Estimate	SD
$\mathcal{D}_e$	[42055.6 cm^{-1}]	Constrained
$n(r)$ function - Ogilvie-Tipping expansion		
r_e	1.20752476624 Å	7.0×10^{-8} Å
ρ_0	3.2038495616	2.5×10^{-6}
ρ_1	1.91640907	9.8×10^{-5}
ρ_2	2.1806630	4.9×10^{-4}
ρ_3	5.99214	4.6×10^{-2}
ρ_4	-1.67857×10^1	1.6×10^{-1}
ρ_5	1.04850×10^1	1.2
ρ_6	5.85040×10^2	5.7
ρ_7	-1.02118×10^3	2.8×10^1
ρ_8	-1.03271×10^4	1.4×10^2
ρ_9	5.13159×10^4	3.2×10^2
ρ_{10}	-5.24653×10^4	1.8×10^3
ρ_{11}	-2.87460×10^5	3.8×10^3
ρ_{12}	1.28986×10^6	7.9×10^3
ρ_{13}	-2.42989×10^6	2.1×10^4
ρ_{14}	2.28313×10^6	2.5×10^4
ρ_{15}	-8.58258×10^5	1.0×10^4
$\alpha(r)$ function - Dunham expansion		
α_4	−4.19459	1.3×10^{-1}
α_5	4.29223×10^1	6.4×10^{-1}
α_6	-3.29590×10^2	1.3
α_7	1.25590×10^3	1.3×10^1
α_8	-2.30370×10^3	3.6×10^1
α_9	1.73434×10^3	4.3×10^1
α_{10}	-2.85625×10^2	1.9×10^1

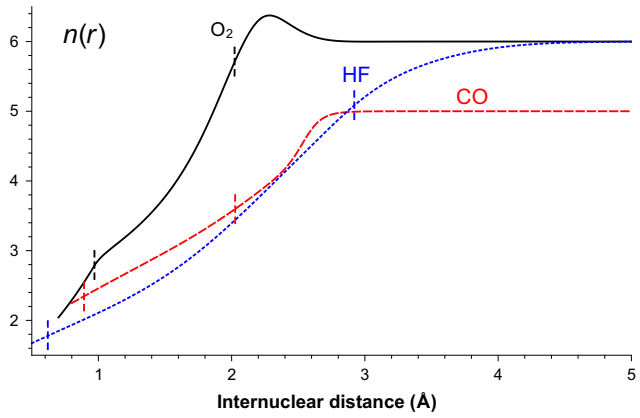


Fig. 1. The $n(r)$ functions for the ground $X^3\Sigma_g^-$ electronic state of O_2, the ground $X^1\Sigma^+$ electronic state of CO, and the ground $X^1\Sigma^+$ electronic state of HF as calculated from the fitted parameters in Tables 1–3, respectively, and the constrained parameters in Table 4. The two short vertical dashed lines on each curve represent the inner and outer classical turning points of the highest observed vibrational level.

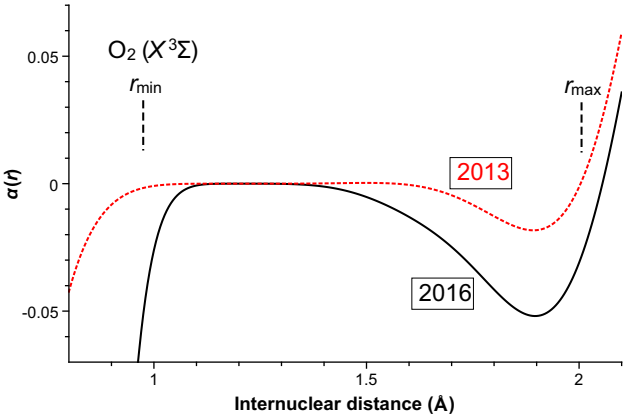


Fig. 2. The $\alpha(r)$ function for the ground $X^3\Sigma_g^-$ electronic state of O_2 as calculated from the fitted parameters in Table 1 and the constrained parameters in Table 4. The black continuous line represents the function obtained in the present work, and the red dashed line represents the analogous function obtained in Ref. [47]. The quantities r_{min} and r_{max} represent the inner and outer classical turning points, respectively, of the highest observed vibrational level.

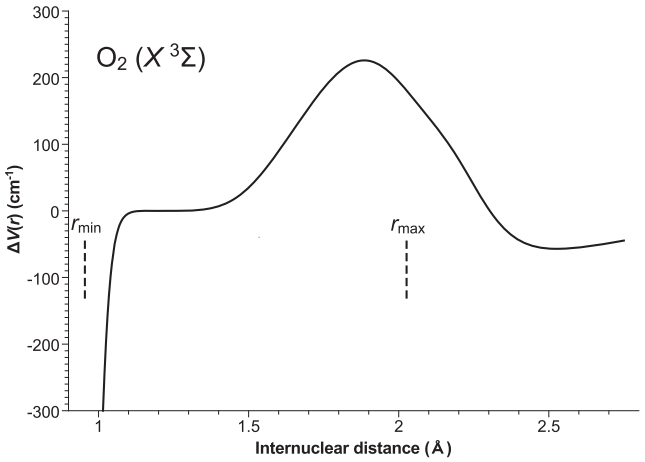


Fig. 3. The $\Delta V(r)$ potential difference function for the ground $X^3\Sigma_g^-$ electronic state of O_2, which is calculated as $\Delta V(r) = V_{2016}(r) - V_{2013}(r)$, where $V_{2016}(r)$ is the ELJ PEF obtained in the present work and $V_{2013}(r)$ is the Morse-like PEF obtained in Ref. [47]. The quantities r_{min} and r_{max} represent the inner and outer classical turning points, respectively, of the highest observed vibrational level.

4.2. The ground $X^1\Sigma^+$ electronic state of CO

A collection of 14,177 pure rotational and vibrational-rotational spectroscopic line positions for the principal isotopologue $^{12}C^{16}O$ was employed in a weighted nonlinear least-squares fit to $V(r)$ and $\alpha(r)$. The weights of the spectroscopic line positions were defined as $1/\varepsilon_i^2$ where ε_i is the experimental uncertainty of the ith line position. This data set is identical to the $^{12}C^{16}O$ subset employed in a multi-isotopologue fit to the MLJ potential function by Coxon and Hajigeorgiou [33] in 2004. The vibrational energies cover approximately 75% of the well depth of the ground state PEF. Radial functions were modeled using polynomial expansions in the Ogilvie-Tipping variable over the radial range 0.80 Å $\leqslant r \leqslant$ 2.40 Å, using a radial mesh size of 0.0004 Å, which are the same as those employed in Ref. [33]. The inner and outer classical turning points for $\upsilon = 41$, the highest observed vibrational level, are 0.86 Å and 1.97 Å, respectively.

The dimensionless reduced standard deviation and root-mean-square deviation (RMS) of the ELJ fit is $\sigma_d = 0.5582$ (RMS = 0.5578). This is in good agreement with the value RMS = 0.5408 obtained in Ref. [33] for the $^{12}C^{16}O$ isotopologue. The MLJ representation of Ref. [33] actually required four fewer parameters than the current ELJ fit, but only a C_5/r^5 term was employed for the long-range region in the former fit, whereas the current ELJ fit employed the long-range expression,

$$V(r) = \mathcal{D}_e - \frac{C_5}{r^5} - \frac{C_6}{r^6}, \tag{16}$$

using $C_5 = 113{,}112$ Å^5 cm^{-1} and $C_6 = 124{,}822$ Å^6 cm^{-1} obtained from the matrix elements of Rerat et al. [49].

Table 2 lists the parameter set corresponding to the ELJ/$\alpha(r)$ fit from the present work. The set of constrained parameters is given in Table 4. Fig. 1 shows the $n(r)$ function and Fig. 4 shows the $\alpha(r)$ function for the $^{12}C^{16}O$ isotopologue obtained in this work. It is of interest to comment on the comparison in Fig. 4 between the current $\alpha(r)$ function with the entirely equivalent 2004 $q(r)$ function from Ref. [33]. The agreement between the two radial functions is very satisfactory in the range 1.0 Å $\leqslant r \leqslant$ 1.8 Å. The increasing deviation for $r >$ 1.8 Å is entirely due to the choice in the present work to dampen $\alpha(r)$ to a limiting value of zero at dissociation, as explained in Section 4.1 above. This approach had not been followed in Ref. [33], leading to a $q(r)$ function with unrealistically increasing negative magnitude at large r. Finally, Fig. 5 shows the potential difference function $\Delta V(r)$ between the present work and Ref. [33]. It is clear that the observed discrepancies at large-r begin to increase dramatically beyond the outermost classical turning point, indicating significant differences in how the long-range portion of the ELJ and MLJ potentials were handled. It is worth emphasizing that a wide range of values δ_{LR} (6.0–8.0) and R_{LR} values (2.70–3.10 Å) were experimented with for the ELJ potential, leading always to insignificant differences in the long-range form. This indicates that the two-term dispersion energy dependence of Eq. (16) gives consistently the same long-range potential. The abrupt increase in $\Delta V(r)$ for $r >$ 2 Å could indicate that use of the leading C_5/r^5 term alone in Ref. [33] gives a poorer representation of the long-range portion of the CO potential.

Table 2
ELJ potential parameters for the $X^1\Sigma^+$ electronic state of CO.

Parameter	Estimate	SD
$\mathcal{D}_e$	[90,674 cm^{-1}]	Constrained
$n(r)$ function - Ogilvie-Tipping expansion		
r_e	1.128322531930 Å	2.6×10^{-10} Å
ρ_0	2.592554289154	1.1×10^{-9}
ρ_1	1.1609997201	1.8×10^{-7}
ρ_2	$5.2412372427 \times 10^{-1}$	3.3×10^{-7}
ρ_3	$3.6614162513 \times 10^{-1}$	2.5×10^{-6}
ρ_4	$3.6945808745 \times 10^{-1}$	5.0×10^{-6}
ρ_5	$7.221044786 \times 10^{-1}$	1.9×10^{-5}
ρ_6	$8.910983457 \times 10^{-1}$	2.5×10^{-5}
ρ_7	1.226907435	4.5×10^{-5}
ρ_8	$4.055633480 \times 10^{-1}$	1.1×10^{-5}
ρ_9	$-2.248557034 \times 10^{1}$	4.0×10^{-4}
ρ_{10}	4.22326463×10^{1}	1.1×10^{-4}
ρ_{11}	1.12448063×10^{2}	4.0×10^{-3}
ρ_{12}	$-6.65662011 \times 10^{2}$	1.5×10^{-2}
ρ_{13}	1.2660188×10^{3}	2.3×10^{-2}
ρ_{14}	-1.0950463×10^{3}	2.2×10^{-2}
ρ_{15}	3.5004062×10^{2}	2.2×10^{-2}
$\alpha(r)$ function - Ogilvie-Tipping expansion		
α_1	-2.532641×10^{-4}	2.3×10^{-7}
α_2	-3.697588×10^{-4}	4.2×10^{-7}
α_3	5.470980×10^{-4}	6.3×10^{-7}
α_4	1.524826×10^{-4}	1.2×10^{-6}

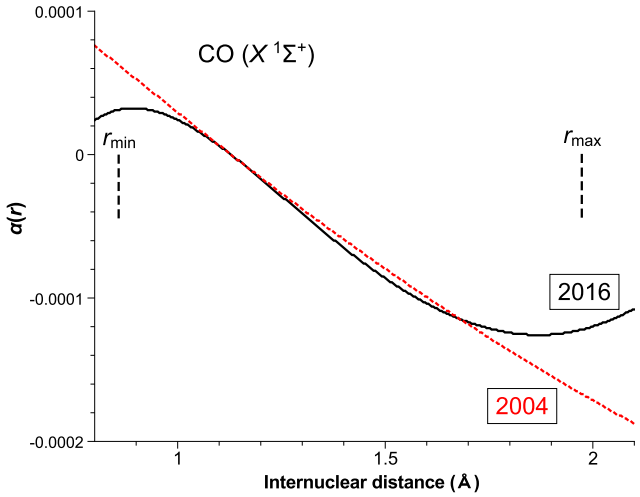


Fig. 4. The $\alpha(r)$ function for the ground $X^1\Sigma^+$ electronic state of CO as calculated from the fitted parameters in Table 2 and the constrained parameters in Table 4. The black continuous line represents the function obtained in the present work, and the red dashed line represents the analogous $q(r)$ function obtained in Ref. [33]. The quantities r_{min} and r_{max} represent the inner and outer classical turning points, respectively, of the highest observed vibrational level.

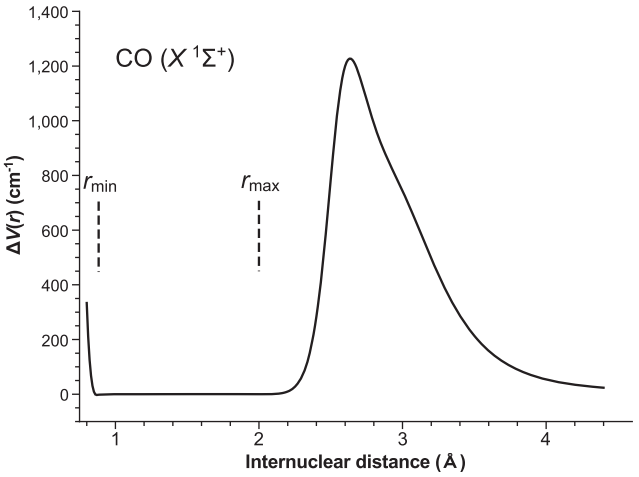


Fig. 5. The $\Delta V(r)$ potential difference function for the ground $X^1\Sigma^+$ electronic state of CO, which is calculated as $\Delta V(r) = V_{2016}(r) - V_{2006}(r)$, where $V_{2016}(r)$ is the ELJ PEF obtained in the present work and $V_{2006}(r)$ is the MLJ PEF obtained in Ref. [33]. The inset on the upper right corner is an expanded view of a narrower section of the $\Delta V(r)$ potential difference function. The quantities r_{min} and r_{max} represent the inner and outer classical turning points, respectively, of the highest observed vibrational level.

It is of interest to compare the equilibrium internuclear separations obtained herein and in past work. In the present work, the estimate $r_e = 1.1283225319(3)$ Å was obtained for the isotopologue $^{12}C^{16}O$, whereas Coxon and Hajigeorgiou [33] reported the estimate $r_e = 1.1283225284(3)$ Å. The difference in the two values, $\Delta r_e = 0.0000000035$ Å is much larger than the combined uncertainties. There are four reasons for this discrepancy: (a) model dependence, (b) the estimate of Ref. [33] resulted from a multi-isotopologue fit, such that the estimated r_e value had to satisfy the spectroscopic information for all isotopologues, not just $^{12}C^{16}O$, (c) a slightly different set of fundamental physicochemical constants was employed in Ref. [33] ($\hbar^2/2 = 16.85762909$ u Å^2 versus $\hbar^2/2 = 16.85762920$ u Å^2 in the present work), and (d) a small difference in the reduced molecular masses employed ($\mu = 6.856208638$ u in Ref. [33], versus $\mu = 6.856208640$ u in the present work). In view of these considerations, the agreement is satisfactory.

4.3. The ground $X^1\Sigma^+$ electronic state of HF

The data set for the ground electronic state of HF comprises a total of 3252 spectroscopic line positions that include pure rotational, vibrational-rotational and electronic ($B^1\Sigma^+ \rightarrow X^1\Sigma^+$) transitions, covering approximately 99.3% of the well depth in vibrational energy. Radial functions were determined in the interval 0.40 Å $\leqslant r \leqslant$ 8.40 Å, using a grid spacing of 0.0005 Å. These values are identical to those employed in the 2015 [14] fit. The HF data set employed recently by Coxon and Hajigeorgiou [14] included 3226 spectroscopic line positions, 26 fewer than that of the current data set. The discrepancy is related to spectroscopic transitions that were excluded in Ref. [14] due to residuals between the observed and calculated line positions that exceeded three standard errors, but that could be included in the current fit to the ELJ model. This difference is expected to lend slightly increased reliability to the radial functions determined in the present work, but also increase the standard deviation of the fit.

In 2006, Coxon and Hajigeorgiou [34] had performed a fit to the PEF of the ground electronic state of HF by considering multi-isotopologue data, using the MLJ potential model. In that work, a total of 17 fitted parameters were required to define the PEF for this electronic state. By contrast, the more recent 2015 fit by Coxon and Hajigeorgiou [14] required a total of 33 fitted parameters to represent the same PEF. It is thought that the drastic difference in the required number of PEF parameters is related to the use of more complicated models in the 2015 fit. Specifically, this relates both to the PEF potential model (MLR3) and the isotopically invariant function $U_H(r)$ (see Ref. [14]). In any case, an important objective of DPF analysis is to employ as small a parameter set as possible. Table 3 lists the parameter set required to define the HF ELJ/$\alpha(r)$ radial functions. The set of constrained parameters is given in Table 4. In the current work, the representation of the HF ELJ model required 17 fitted parameters, exactly the same as the 2006 MLJ fit. Dunham polynomial representations were employed both for the $n(r)$ and $\alpha(r)$ ($q(r)$) radial functions.

In both the 2006 [34] and 2015 [14] DPF analyses, the PEF of the $B^1\Sigma^+$ electronic state of HF had also been fitted directly. In the present work, since the emphasis was on the PEF of the ground electronic state, the fit involved constraining the energy term values for the $B^1\Sigma^+$ electronic state to the set published recently [14].

Table 3
ELJ potential parameters for the $X^1\Sigma^+$ electronic state of HF.

Parameter	Estimate	SD
$\mathcal{D}_e$	[49361.6 cm^{-1}]	Constrained
$n(r)$ function - Dunham expansion		
r_e	0.91683896366 Å	1.5×10^{-8} Å
ρ_0	2.0346549019	2.4×10^{-7}
ρ_1	$8.023130326 \times 10^{-1}$	7.4×10^{-6}
ρ_2	$1.02189123 \times 10^{-1}$	2.2×10^{-5}
ρ_3	$2.13449099 \times 10^{-1}$	1.2×10^{-4}
ρ_4	$-5.33673320 \times 10^{-2}$	4.0×10^{-4}
ρ_5	4.5222725×10^{-2}	2.0×10^{-3}
ρ_6	-1.076711×10^{-1}	3.7×10^{-3}
ρ_7	1.547787×10^{-1}	1.1×10^{-2}
ρ_8	3.339251×10^{-1}	3.3×10^{-2}
ρ_9	-1.745053	4.4×10^{-2}
ρ_{10}	3.154700	2.7×10^{-2}
ρ_{11}	-3.229448	2.3×10^{-3}
ρ_{12}	2.033251	1.0×10^{-2}
ρ_{13}	-7.803793×10^{-1}	6.8×10^{-3}
ρ_{14}	1.678004×10^{-1}	1.9×10^{-3}
ρ_{15}	-1.563306×10^{-2}	2.1×10^{-4}
$\alpha(r)$ function - Dunham expansion		
α_1	-6.875509×10^{-5}	1.7×10^{-6}
α_2	-6.297063×10^{-4}	2.3×10^{-5}
α_3	2.031582×10^{-4}	5.1×10^{-5}
α_4	2.970436×10^{-4}	1.1×10^{-4}
α_5	-1.128898×10^{-3}	1.7×10^{-4}
α_6	5.874624×10^{-4}	1.1×10^{-4}
α_7	-2.026593×10^{-4}	2.3×10^{-5}
$\delta\Delta T_e$	7.459×10^{-2} cm^{-1}	3.1×10^{-3} cm^1

Table 4
Constrained ELJ potential parameters.

Parameter	O_2 ($X^3\Sigma_g^-$)	CO ($X^1\Sigma^+$)	HF ($X^1\Sigma^+$)
Eq. (5)			
δ_n (Å^{-1})	14.0	15.0	9.0
R_n (Å)	2.19	2.55	2.60
Eq. (9)			
δ_{LR} (Å^{-1})	8.0	8.0	8.0
R_{LR} (Å)	2.32	2.90	3.15
Eq. (14)			
δ_α (Å^{-1})	8.0	5.0	0.9
R_α (Å)	1.70	2.30	2.85
Eq. (10)			
a	0.91199252	1.55292286	1.29868417
b (Å^{-1})	1.15137338	0.46246693	0.50644352
R_c (Å)	0.9645	0.87	0.60

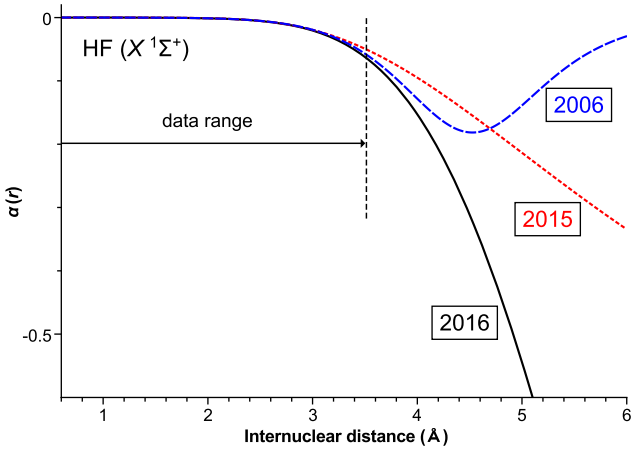


Fig. 6. The $\alpha(r)$ function for the ground $X^1\Sigma^+$ electronic state of HF as calculated from the fitted parameters in Table 3 and the constrained parameters in Table 4. The black continuous line represents the function obtained in the present work, the red short-dashed line represents the analogous $q(r)$ function obtained in Ref. [14], and the blue long-dashed line represents the analogous $q(r)$ function obtained in Ref. [34].

The quantity $\delta\Delta T_e$ represents a constant shift from the electronic term value of the $B^1\Sigma^+$ electronic state, and was found to be significantly determined in the present work.

Fig. 1 shows the $n(r)$ function obtained in the present work, and Fig. 6 shows the $\alpha(r)$ function from the present DPF fit. For the latter, there is a comparison with the completely analogous 2015 $q(r)$ function [14], and the 2006 $q(r)$ function [34]. It is obvious that the agreement between the three functions is very satisfactory in the range covered by the data, but beyond this region there are significant, yet largely inconsequential, differences. Fig. 7 shows the potential difference function $\Delta V(r)$ between the present work and Ref. [14]. It is seen in Fig. 7, that the potential difference function between the ELJ and MLR3 functions is quite reasonable, particularly over the inner and outer classical turning points (0.62 Å and 2.87 Å, respectively) for $\upsilon = 19$, the highest observed level. The oscillatory nature of $\Delta V(r)$ at large-r is likely due to the very high degree polynomial employed in Ref. [14], and the different

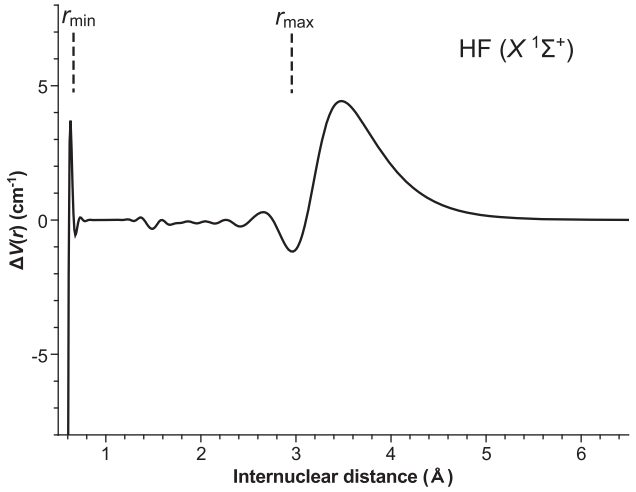


Fig. 7. The $\Delta V(r)$ potential difference function for the ground $X^1\Sigma^+$ electronic state of HF, which is calculated as $\Delta V(r) = V_{2016}(r) - V_{2015}(r)$, where $V_{2016}(r)$ is the ELJ PEF obtained in the present work and $V_{2015}(r)$ is the MLR3 PEF obtained in Ref. [14]. The quantities r_{min} and r_{max} represent the inner and outer classical turning points, respectively, of the highest observed vibrational level.

way in which the long-range dispersion term damping is handled in the two analyses.

The dimensionless reduced standard deviation obtained in the present fit is $\sigma_d = 1.0381$ (RMS = 1.0328), which compares well with the RMS = 0.9862 obtained in the most recent DPF analysis [14]. The present value is slightly higher because of the inclusion of 26 additional spectroscopic line positions having generally higher residuals. The estimate $r_e = 0.91683896(1)$ Å obtained in the current DPF fit, is in excellent agreement with the estimate from the 2015 DPF analysis, $r_e = 0.91683897(4)$ Å, which was obtained by considering only lower-υ spectroscopic data, and with the full-υ 2006 estimate, $r_e = 0.91683896(2)$ Å.

The long-range region model employed in the current fit is identical in form to Eq. (15). The estimates employed in the present work are $C_6 = 31{,}755$ Å^6 cm^{-1}, $C_8 = 1.667 \times 10^5$ Å^8 cm^{-1} and $C_{10} = 1.125 \times 10^6$ Å^{10} cm^{-1}, which are ab initio estimates from the work of Zatsarinni et al. [51]. These were also employed in the 2015 DPF fit [14], but the 2006 DPF fit [34], which was based on the simpler MLJ model, included only the leading inverse-power C_6/r^6 term and employed an older and less accurate C_6 constant [52].

5. Discussion and conclusions

In the present work, a modified version of the potential model of Hajigeorgiou [16] was employed in DPF analyses of the ground electronic states of O_2, CO and HF. The principal objective of the present work was to demonstrate that the ELJ model can lead to simple, reliable, and compact representations of the PEF of a single electronic state of a single isotopologue. The scenarios of including more electronic states and more isotopologues in simultaneous DPF fits will be explored in future work. Insofar as simplicity in the models of all radial functions will be sought, it is not expected that these investigations will change significantly the main conclusions reached in the present work.

In terms of compactness, the ELJ model demonstrated performance very similar to the equally simple MLJ model. However, the ELJ model can accommodate a multi-term dispersion energy coefficient set, whereas the MLJ model is fundamentally restricted to include only the leading inverse-power dispersion energy term. This can be considered the greatest advantage of the ELJ model over the MLJ model. The simple MLR model, which does not include dispersion damping functions, suffers from problems on the inner limb due to runaway inverse-power terms at short-r. This is not the case for the ELJ model proposed herein. In terms of reliability, the ELJ model produced PEFs that are in very good agreement with those obtained in previous work using other types of mathematical models, some of which are more complicated in form and can lead to less compact representations. An additional positive feature of the ELJ model is that it inherently involves less experimentation and fine-tuning at the fitting stage compared to the MLR/MLR3 models, owing to the use of simpler polynomial expansion variables, such as those of Dunham and Ogilvie-Tipping. The use of Šurkus-like variables in MLR/MLR3 analyses, the use of a manually adjustable pivot point different than r_e for some polynomial expansions, as well as the additional option to have different numbers of terms for the inner and outer limbs for the various radial functions, requires significantly more testing in converging to the best representations.

As stated earlier, the long-range damping function parameters δ_{LR} and R_{LR} in Eq. (9) are adjusted manually by reference to the standard deviation of the least-squares fit. However, this is not the sole criterion for making adjustments to the long-range potential region. A critical test of the reliability of the long-range portions of the derived PEFs and of their ability to extrapolate

dependably consists of constructing and examining "Le Roy" limiting long-range diagrams. For both O_2 and HF, the long-range PEFs were represented by the expression Eq. (15). This expression can be transformed as in,

$$C_6^{\text{eff}}(r) = r^6[\mathcal{D}_e - V(r)] = C_6 + \frac{C_8}{r^2} + \frac{C_{10}}{r^4}, \tag{17}$$

$$C_8^{\text{eff}}(r) = r^8\left[\mathcal{D}_e - V(r) - \frac{C_6}{r^6}\right] = C_8 + \frac{C_{10}}{r^2}, \tag{18}$$

$$C_{10}^{\text{eff}}(r) = r^{10}\left[\mathcal{D}_e - V(r) - \frac{C_6}{r^6} - \frac{C_8}{r^8}\right] = C_{10}, \tag{19}$$

and in each case a plot should be made with the left-hand-side of Eqs. (17)–(19) as the ordinate and the function $1/r^2$ as the abscissa. In making such a plot for Eq. (17), for example, the ordinate intersection point where the abscissa is equal to zero (very large r) should be equal to C_6 and the slope of the limiting ($r \to \infty$) curve should be equal to C_8.

These diagrams are shown for the ground $X^1\Sigma^+$ electronic state of HF in Figs. 8–10 for Eqs. (17)–(19), respectively. Similar diagrams are constructed for O_2, shown in Figs. 12–14 inclusive, and for CO in Figs. 15 and 16. Figs. 12–16 are given as Supplementary material. The diagrams shown for O_2 and HF are very satisfactory indicating that the PEFs for these molecules should have dependable extrapolation properties to higher energy. For CO, the analogous diagrams are reasonable though not quite as aesthetically pleasing as in the cases of O_2 and HF. They do, nevertheless, satisfy the long-range conditions. These observations for CO may be related to the much wider extrapolation from the highest observed vibrational level to the dissociation limit for this diatomic molecule than what is the case for O_2 and HF, and also because of the fact that two dispersion coefficients (C_5 and C_6) were employed only.

A crucial observation is made in examining the two plots of Eq. (19) for HF and O_2 and the analogous plot for CO (Figs. 10, 14 and 16 respectively). The limiting slopes ($r \to \infty$) of the curves are exactly zero. This is a clear indication that no implicit higher-order inverse-power terms are generated for the ELJ model. This is not the case for the MLR/MLR3 models, where it is found that implicit terms beyond the order employed explicitly are generated because of the very structure of the models. Specifically, the dispersion term damping functions employed in these models do not tend to zero fast enough as $r \to 0$, whereas for the ELJ model

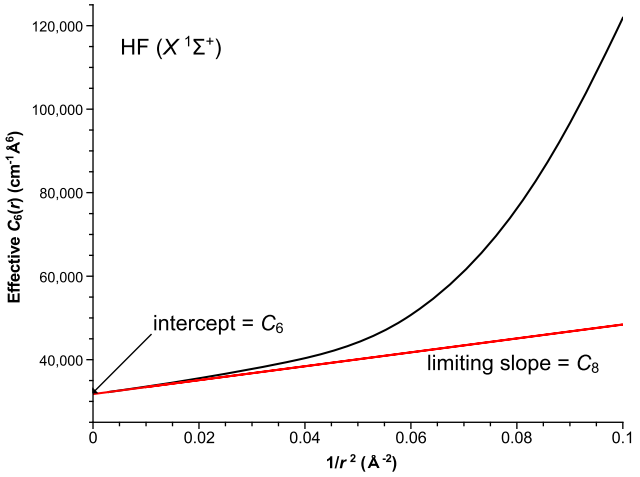


Fig. 8. Limiting long-range diagram for the ground $X^1\Sigma^+$ electronic state of HF. The solid line shows the function $C_6^{\text{eff}}(r) = r^6[D_e - V(r)]$ plotted versus $1/r^2$ (see text, Eq. (17)) using the fitted ELJ potential obtained in this work. The red line represents the term $C_6 + C_8/r^2$ calculated from the theoretical dispersion constants of Ref. [51].

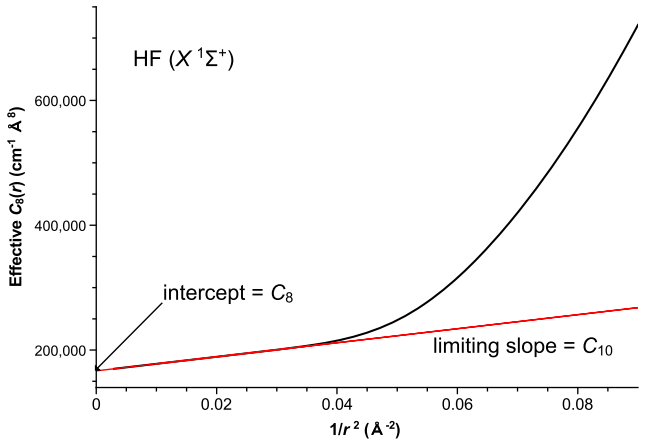


Fig. 9. Limiting long-range diagram for the ground $X^1\Sigma^+$ electronic state of HF. The solid line shows the function $C_8^{\text{eff}}(r) = r^8[D_e - V(r) - C_6/r^6]$ plotted versus $1/r^2$ (see text, Eq. (18)) using the fitted ELJ potential. The red line represents the term $C_8 + C_{10}/r^2$ calculated from the theoretical dispersion constants of Ref. [51].

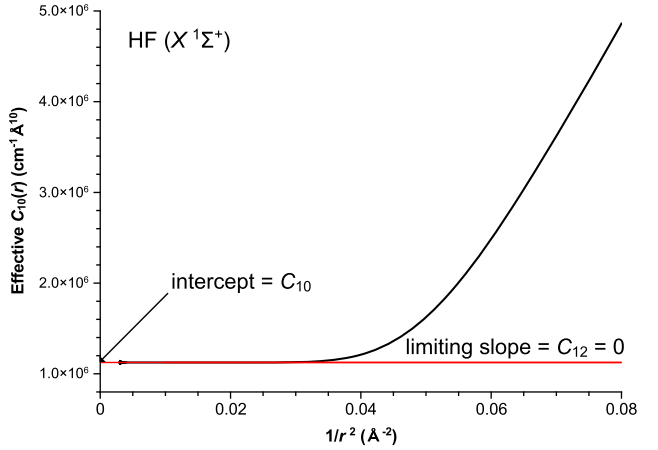


Fig. 10. Limiting long-range diagram for the ground $X^1\Sigma^+$ electronic state of HF. The solid line shows the function $C_{10}^{\text{eff}}(r) = r^{10}[D_e - V(r) - C_6/r^6 - C_8/r^8]$ plotted versus $1/r^2$ (see text, Eq. (19)) using the fitted ELJ potential. The red horizontal line represents the constant term C_{10} obtained from Ref. [51]. The limiting ($r \to \infty$) slope of zero of the black curve indicates that there are no implicit higher-order terms inherent in the ELJ model (see text).

the collective empirical damping function $f_{LR}(r)/f_{LR}(r_e)$ in Eq. (7) ensures that these terms disappear completely for $r \leqslant r_e$. The MLR/MLR3 finite implicit terms are often completely inconsistent with the expected values of the higher-order dispersion coefficients, although a simple MLR3 adaptation by Coxon and Hajigeorgiou [14] has made it possible to reproduce the theoretical value of the first implicit higher-order dispersion coefficient. However, it must be made clear that the presence of such implicit terms for the MLR/MLR3 models is considered more of an undesirable complication rather than an advantage. In the application of the ELJ model as presented herein, the dispersion energy inverse-power series can be as extensive as desired without causing any short-r problems, and without the need for extensive complicated damping functions for each term. In addition, it can be shown that the individual dispersion term damping functions employed in the MLR/MLR3 models have finite magnitudes at the potential minimum, which may also adversely affect the determination of accurate estimates of the equilibrium internuclear separation, r_e. In the construction of the ELJ model, such damping was adjusted to have no effect at the potential minimum, as discussed previously

following Eqs. (6)–(9). These considerations constitute important advantages of the ELJ form over the MLR/MLR3 models.

It is equally important to draw attention to some of the less positive features of the ELJ model, as ascertained in the present work. One undesirable characteristic is the necessity to control directly the inner limb behavior through the methodology inherent in Eq. (10), and discussed further in Section 3 above. This is an inevitable consequence of employing high powers in the polynomial expansion for $n(r)$ in order to achieve success in representing highly precise spectroscopic data to within the experimental uncertainties. In the future, the approach of using an expansion point other than r_e in Eq. (4), such as the R_{ref} approach used in MLR/MLR3 fits, will be investigated. This approach has been shown to reduce the number of polynomial terms required for a satisfactory fit, and this would reduce the possibility of unreasonable behavior in $n(r)$ for the inner limb. Another feature that may be considered less than desirable is the use of a collective damping function for all dispersion energy terms in Eq. (7). This approach has been employed also by other authors [53–55] in similar type of work, but the alternative approach of applying individual damping functions for each dispersion energy term may be considered more appropriate in terms of theoretical considerations. Specifically, it is expected that as the electron clouds begin to overlap on shorter internuclear separations, the dispersion terms would weaken, but each dispersion term would do so at different rates. It is important to state, however, that the dispersion damping functions employed for the MLR/MLR3 models are generalized extensions derived from numerical hydrogen-hydrogen dispersion damping functions that were calculated by ab initio methods [56]. It has not been demonstrated rigorously that the Douketis-type damping functions [57] would correspond to the proper ab initio calculations beyond hydrogen. In principle, ab initio calculated dispersion damping functions should be employed when atoms other than hydrogen are involved. It would then appear that the damping functions employed for the MLR/MLR3 models are to a certain extent approximations. In any case, aside from the theoretical arguments on which they rest, the principal aim of damping functions is the prevention of erratic behavior in $V(r)$ on the inner limb due to the ordinary poles at $r = 0$ of all dispersion energy inverse-power terms. It is therefore considered that the use of a communal damping function offers significant advantage in terms of the simplicity imparted to the model.

The use of three individual switching functions in the current work may be considered a drawback, particularly as the use of switching functions of the type employed herein has been criticized previously [48] for having ad hoc arbitrary nature. A concomitant objection may be raised due to a perceived requirement of spending a great deal of time in optimizing the parameters of such functions. In defense of switching functions, these are employed widely in chemical physics, and in the present applications precise prescriptions were provided for the selection of initial estimates for the pivot radial distances $R_n/R_{LR}/R_\alpha$ and their associated damping strength parameters $\delta_n/\delta_{LR}/\delta_\alpha$. It must also be emphasized that the switching functions are not entirely independent entities, but are to a certain extent amalgamated with the radial functions to which they are coupled. This makes possible a fairly wide range of acceptable parameter sets for the switching functions, minimizing the time required to optimize the models. In addition, in the present work, it has been clearly demonstrated that the use of switching functions can naturally produce sensible long-range limiting diagrams, without compromising the quality of the fit. At an early stage of testing the ELJ model, sigmoidal switching functions of the type,

$$f_i(r) = \frac{R_i^p}{R_i^p + r^p}, \tag{20}$$

were experimented with, and these bear some resemblance to the Šurkus-like functional forms employed in MLR/MLR3 models. These switching functions were found to give results that were essentially identical to those obtained using the forms finally adopted in this work and thus offer no further advantage. In both cases, there are two adjustable parameters, thus, in principle, either type of sigmoidal switching function could be employed with the ELJ model and the issue is reduced to one of personal preference.

In the application to the ground electronic state of O_2 the potential difference function $\Delta V(r)$ displayed significant magnitude at large-r, most likely due to the introduction in the present work of proper long-range behavior. The positive differences at large-r are accompanied by larger negative differences at short-r, so that the energy term values are reproduced satisfactorily by the combination of $V(r)$ and $\alpha(r)$. This observation may imply a certain degree of non-uniqueness in the fitted radial functions when employing a set of calculated term values as the observables. That is, two different combinations of $V(r)$ and $\alpha(r)$ were found to represent satisfactorily the same set of calculated term values, in the present work and in Ref. [47]. This type of non-uniqueness has been discussed and treated mathematically in Hajigeorgiou's doctoral dissertation [58]. Basically, it was shown therein, using a purely mathematical argument, that there exists, in principle, an infinite number of rotationless internuclear potential functions, having different equilibrium internuclear distances but identical shapes, and that are associated with identical vibrational point spectra. In a similar way, each unique PEF is associated with a unique, and appropriately transformed $\alpha(r)$ function, so that an infinite combination of $V(r)$-$\alpha(r)$ function sets can replicate the same vibrational-rotational eigenvalues. The work of Watson [59] showed that non-uniqueness in the determination of pertinent radial functions does indeed rest on a sound theoretical footing, but a common reference convention was suggested for eliminating the non-uniqueness in applying the arbitrary constraint $\alpha(r_e) = 0$.

As discussed earlier on in Section 4.1, the fitted $n(r)$ function for O_2 displays a real well-defined maximum on the outer limb. A similar maximum in $n(r)$ is also found for the ground $X^1\Sigma_g^+$ electronic state of Cl_2, but it does not appear for HF and CO. It is of interest to discuss the reasons for the appearance of this maximum in $n(r)$. The function $n(r)$ is essentially a collection of "local" effective n values in representing the PEF by Eq. (1). If the outer limb energy rises fairly steeply towards the dissociation limit, the local value of n would be expected to increase. Upon reflection, another way to picture this is by considering the degree of anharmonicity of the PEF. One would expect that the lower the anharmonicity on the outer limb, the higher the local values of n. It is therefore entirely possible that a PEF with a very small degree of outer limb anharmonicity will produce local n values that can exceed the limiting n_1 value in Eq. (2), before eventually settling to the long-range value of n_1. This situation gives rise to a maximum in the $n(r)$ function. In order to assess the relative degree of anharmonicity in PEFs for different electronic states, it is helpful to consider a plot of reduced PEFs, with r/r_e as the abscissa and $V(r)/\mathcal{D}_e$ as the ordinate. This type of plot is shown in Fig. 11. It is very clear that the ground states of Cl_2 and O_2 have relatively small degrees of anharmonicity, and thus display a maximum in their respective $n(r)$ functions. By contrast, the relatively high anharmonicity PEFs of CO and HF are not associated with maxima in $n(r)$ in Fig. 1.

The computer code for performing the analyses described in this article is not adequately generalized at this time to warrant its mass distribution. Investigators interested in having access to this code may contact the author directly.

In conclusion, there appears to be no exclusive mathematical form for representing the PEF of a well-behaved isolated electronic state. One must aim to construct a simple empirical closed-form

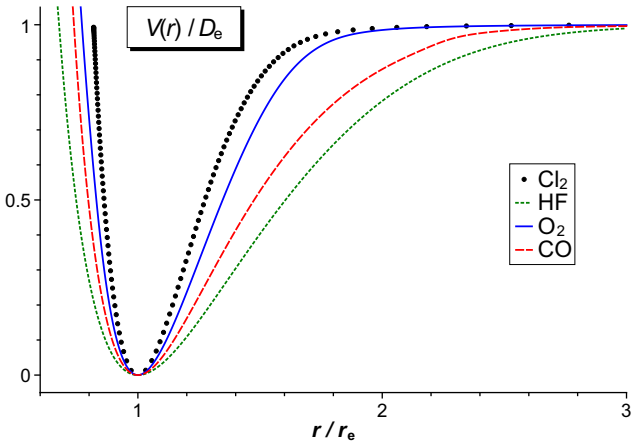


Fig. 11. Reduced internuclear potential energy curves for the ground electronic states of Cl_2, HF, O_2, and CO. For HF, O_2, and CO these curves were calculated from the fitted PEFs obtained in the present work, and for the ground electronic state of Cl_2 the original PEF was obtained from the work of Douglas and Hoy [60].

model, as compact as possible, and replicating as closely as can be reasonably expected the actual physics of a chemical bond. The present work has demonstrated the usefulness of the ELJ model for DPF work in diatomic molecules. The model leads to simple, compact and reliable representations of the PEF and can thus be added to the collection of suitable functions for DPF analysis of diatomic systems. In terms of complexity, it falls somewhere in-between the MLJ and the MLR models. The ELJ model, as demonstrated in the present work, represents a compromise between simplicity and the theoretically known physical behavior of a diatomic internuclear bond.

Acknowledgments

The author wishes to thank the School of Medicine, University of Nicosia for support of this work, and Prof. John Coxon for useful correspondence and for reviewing an earlier version of the manuscript. Prof. Robert Le Roy, who is being honored in this special issue of the journal, is warmly thanked for contributing to the author's early education during a Research Associate position at the University of Waterloo in 1994–1995.

Appendix A. Supplementary data

Supplementary data associated with this article can be found, in the online version, at http://dx.doi.org/10.1016/j.jms.2016.06.014.

References

[1] W. Heisenberg, Z. Phys. 33 (1925) 879–893.
[2] E. Schrödinger, Phys. Rev. 28 (1926) 1049–1070.
[3] A. Kratzer, Z. Phys. 3 (1920) 289–307.
[4] J.E. Jones, Proc. R. Soc. Lond. A 106 (1924) 463–477.
[5] E. Fues, Ann. Phys. 80 (1926) 367–370.
[6] P.M. Morse, Phys. Rev. 34 (1929) 57–64.
[7] M. Born, J.R. Oppenheimer, Ann. Phys. 389 (1927) 457–484.
[8] R. Rydberg, Z. Phys. 73 (1931) 376–385.
[9] O. Klein, Z. Phys. 76 (1932) 226–235.
[10] A.L.G. Rees, Proc. Phys. Soc. (London) 59 (1947) 998–1008.
[11] G. Wentzel, Z. Phys. 38 (1926) 518–529.
[12] H.A. Kramers, Z. Phys. 39 (1926) 828–840.
[13] L. Brillouin, J. Phys. Rad. 7 (1926) 353–368.
[14] J.A. Coxon, P.G. Hajigeorgiou, J. Quant. Spectrosc. Radiat. Transfer 151 (2015) 133–154.
[15] Y.-S. Cho, R.J. Le Roy, J. Chem. Phys. 144 (2016) 024311.
[16] P.G. Hajigeorgiou, J. Mol. Spectrosc. 263 (2010) 101–110; see also Corrigendum, P.G. Hajigeorgiou, J. Mol. Spectrosc. 269 (2011) 141.
[17] M. Gruebele, E. Keim, A. Stein, R.J. Saykally, J. Mol. Spectrosc. 131 (1988) 343–366.
[18] J.L. Dunham, Phys. Rev. 41 (1932) 721–731.
[19] G. Simons, R.G. Parr, J.M. Finlan, J. Chem. Phys. 59 (1973) 3229–3234.
[20] J.A. Coxon, P.G. Hajigeorgiou, J. Mol. Spectrosc. 139 (1990) 84–106.
[21] J.A. Coxon, P.G. Hajigeorgiou, J. Mol. Spectrosc. 150 (1991) 1–27.
[22] J.A. Coxon, P.G. Hajigeorgiou, Can. J. Phys. 70 (1992) 40–53.
[23] J.A. Coxon, P.G. Hajigeorgiou, Chem. Phys. 167 (1992) 327–340.
[24] H.G. Hedderich, M. Dulick, P.F. Bernath, J. Chem. Phys. 99 (1993) 8363–8370.
[25] J.B. White, M. Dulick, P.F. Bernath, J. Chem. Phys. 99 (1993) 8371–8378.
[26] J.M. Campbell, M. Dulick, D. Klapstein, J.B. White, P.F. Bernath, J. Chem. Phys. 99 (1993) 8379–8384.
[27] P.G. Hajigeorgiou, R.J. Le Roy, in: 49th Ohio State University International Symposium on Molecular Spectroscopy, Columbus, Ohio 1994, paper WE04.
[28] R.J. Le Roy, in: R. Barrow (Ed.), Molecular Spectroscopy, vol. 1, Chemical Society of London, London, 1973, pp. 113–176 ((Specialist Periodical Report 3)).
[29] P.G. Hajigeorgiou, R.J. Le Roy, J. Chem. Phys. 112 (2000) 3949–3957.
[30] J.A. Coxon, P.G. Hajigeorgiou, J. Mol. Spectrosc. 193 (1999) 306–318.
[31] J.Y. Seto, R.J. Le Roy, J. Vergès, C. Amiot, J. Chem. Phys. 13 (2000) 3067–3076.
[32] J.A. Coxon, P.G. Hajigeorgiou, J. Mol. Spectrosc. 203 (2000) 49–64.
[33] J.A. Coxon, P.G. Hajigeorgiou, J. Chem. Phys. 121 (2004) 2992–3008.
[34] J.A. Coxon, P.G. Hajigeorgiou, J. Phys. Chem. A 110 (2006) 6261–6270.
[35] R.J. Le Roy, R.D.E. Henderson, Mol. Phys. 105 (2007) 663–677.
[36] J.O. Hirschfelder, W.J. Meath, in: J.O. Hirschfelder (Ed.), Intermolecular Forces, Adv. Chem. Phys., vol. 12, Interscience, New York, 1967, pp. 3–106.
[37] R.J. Le Roy, Y. Huang, C. Jary, J. Chem. Phys. 125 (2006) 164310.
[38] H. Salami, A.J. Ross, P. Crozet, W. Jastrzebski, P. Kowalczyk, R.J. Le Roy, J. Chem. Phys. 126 (2007) 194313.
[39] A. Shayesteh, R.D.E. Henderson, R.J. Le Roy, P.F. Bernath, J. Phys. Chem. A 111 (2007) 2495–12505.
[40] H. Li, R.J. Le Roy, Phys. Chem. Chem. Phys. 10 (2008) 4128–4137.
[41] R.J. Le Roy, N. Dattani, J.A. Coxon, A.J. Ross, P. Crozet, C. Linton, J. Chem. Phys. 131 (2009) 204309.
[42] H. Li, P.-N. Roy, R.J. Le Roy, J. Chem. Phys. 132 (2010) 214309.
[43] J.A. Coxon, P.G. Hajigeorgiou, J. Chem. Phys. 132 (2010) 094105.
[44] R.J. Le Roy, C.C. Haugen, J. Tao, H. Li, Mol. Phys. 109 (2011) 435–446.
[45] J.F. Ogilvie, Proc. R. Soc. Lond., Ser. A 378 (1981) 287–300.
[46] R.J. Le Roy, Can. J. Phys. 52 (1974) 246–256.
[47] P.G. Hajigeorgiou, J. Chem. Phys. 138 (2013) 014309.
[48] Y. Huang, R.J. Le Roy, J. Mol. Struct. Theochem. 591 (2002) 175–187.
[49] M. Rérat, B. Bussery, M. Frécon, J. Mol. Spectrosc. 182 (1997) 260–270.
[50] A.J.C. Varandas, Adv. Chem. Phys. 74 (1988) 255–401.
[51] O. Zatsarinny, K. Bartschat, J. Mitroy, J.-Y. Zhang, J. Chem. Phys. 130 (2009) 124310.
[52] W.T. Zemke, W.C. Stwalley, J.A. Coxon, P.G. Hajigeorgiou, Chem. Phys. Lett. 177 (1991) 412–418.
[53] R. Ahlrichs, R. Penco, G. Scoles, Chem. Phys. 19 (1977) 119–130.
[54] R.A. Aziz, H.H. Chen, J. Chem. Phys. 67 (1977) 5719–5726.
[55] P. Huxley, P.B. Knowles, J.N. Murrell, J.D. Watts, J. Chem. Soc. Faraday Trans. 2 (80) (1984) 1349–1361.
[56] H. Kreek, W.J. Meath, J. Chem. Phys. 50 (1969) 2289–2301.
[57] C. Douketis, G. Scoles, S. Marchetti, M. Zen, A.J. Thakkar, J. Chem. Phys. 76 (1982) 3057–3063.
[58] P.G. Hajigeorgiou, Ph.D. Dissertation, Dalhousie University, 1990, pp. 246–252.
[59] J.K.G. Watson, J. Mol. Spectrosc. 80 (1980) 411–421.
[60] A.E. Douglas, A.R. Hoy, Can. J. Phys. 53 (1975) 1965–1975.